Formation of current filaments in *n*-type GaAs under crossed electric and magnetic fields

Kazuaki Kunihiro,* Michael Gaa, and Eckehard Schöll
Institut für Theoretische Physik, Technische Universität Berlin, Hardenbergstrasse 36, 10623 Berlin, Germany
(Received 14 June 1996; revised manuscript received 13 September 1996)

We present two-dimensional simulations of current filaments in the regime of low-temperature impurity breakdown in thin *n*-GaAs films under the influence of a magnetic field perpendicular to the sample plane. Our simulations show that current filaments are bent by the Lorentz force and their width and curvature increase with magnetic-field strength. Significant asymmetry of the electric fields is observed at opposite filament boundaries. These results agree well with experiments. It is also revealed by simulations that impurity breakdown is accelerated by the presence of an external magnetic field. This is attributed to a finite Hall field inside the filaments. [S0163-1829(97)00203-8]

I. INTRODUCTION

At low temperatures impact ionization of shallow impurities induces a nonequilibrium phase transition in high-purity semiconductors which changes the sample state drastically from a nearly insulating phase to a highly conducting phase, when the electric field exceeds a critical value. In this phenomenon, *S*-shaped negative differential conductivity and self-organized current filaments, i.e., spatially inhomogeneous current flow, are often observed, accompanied by a variety of spatiotemporal instabilities. Steady state and dynamical properties of impurity breakdown have been modeled in the framework of nonlinear generation-recombination (GR) processes,[1–11] and investigated experimentally in various materials.

In the breakdown regime, self-sustained periodic and complex chaotic oscillations have often been observed under dc bias,[12–19] and the spatial patterns of current filaments have been imaged by different techniques, such as scanning electron microscopy,[20] scanning laser microscopy,[8,21,22] and quenched photoluminescence measurement.[23] Among these experimental investigations, some have revealed that applying a magnetic field perpendicular to the electric field significantly changes the spatiotemporal behavior involved in the breakdown regime. For instance, it has been observed that even a relatively weak magnetic field can induce complex chaotic current oscillations,[14–19] current filaments traveling transversally,[24] and filaments spatially deformed by the Lorentz force.[8,21,22]

Some theoretical work has also been carried out to investigate the effects of a magnetic field in the breakdown regime. The dynamic Hall effect has been proposed as a mechanism to induce chaotic temporal oscillations.[25] The transverse periodic or chaotic motion of a current filament under crossed electric and magnetic field has been numerically analyzed by one-dimensional simulations based on the semiclassical semiconductor-transport equations neglecting the longitudinal spatial dependence.[26] A simple phenomenological approach, which focused on the local interaction between different regions of a filament and ignored overall carrier transport and space charges, has been used to reproduce chaotic oscillations found in experiments.[27] In addition, the spatial deformation of current filaments in the presence of a transverse magnetic field has been explained by an effectively one-dimensional drift-diffusion model assuming a dipolelike electric field between two point contacts.[8] However, in order to fully understand the effects of a transverse magnetic field on the filament properties, two-dimensional (2D) analyses including the spatial dependence on both the longitudinal x- and the transverse z direction are indispensable since the Lorentz force acts on charge-carriers moving between the contacts, and points in the direction perpendicular to their motion.

In this paper, we perform 2D simulations of the formation of current filaments in *n*-type GaAs under a transverse magnetic field, and obtain filaments bent by the Lorentz force showing a strong asymmetry of the electric-field strength at opposite filament boundaries. Our simulations are based on the semiclassical equations of macroscopic carrier transport in semiconductors combined with GR rates which are obtained by fitting microscopic Monte Carlo (MC) data. Thereby we gain a much more detailed microscopic understanding than by the phenomenological GR rates used previously.[8,25,27]

This paper is organized as follows. In Sec. II the constitutive model equations are briefly described. In Sec. III we present the simulation results for the formation of current filaments bent by the Lorentz force. We discuss the results in Sec. IV, and finally draw some conclusions in Sec. V.

II. THE MODEL

The basic equations used in the numerical simulations for impurity breakdown in *n*-type partially compensated GaAs have been given in Ref. 11. The experimentally observed bistability in the breakdown regime can be explained in terms of standard GR kinetics including impact ionization only if at least two donor levels, i.e., ground state and excited state, are taken into account.[1,2] We describe the states by the spatial distribution of the carrier density in the conduction band $n(x,z,t)$, in the donor ground level $n_1(x,z,t)$, and in the donor excited level $n_2(x,z,t)$ as well as the local electric field $\mathcal{E}(x,z,t)$, where x and z denote the spatial coordinates parallel and perpendicular to the direction of the applied field, and t is time.

The temporal evolution of the system is governed by rate

equations for n, n_1, and n_2, including impact ionization from the ground and excited level, capture and thermal ionization of the excited level, and transitions between the ground level and the excited level. These GR rates are obtained self-consistently from stationary spatially homogeneous MC simulations by averaging the microscopic transition probabilities over the nonequilibrium distribution function which is extracted from the MC data.[9] They depend on the local field as well as on the carrier densities, and can be parametrized by the local electron temperature $T_e(\mathcal{E},n)$ defined by the variance of the nonequilibrium distribution function. These MC data are represented by fit functions to be adopted into the numerical scheme.[11] This approach serves to combine the microscopic physics of carrier scattering and GR processes and the macroscopic nonlinear spatiotemporal dynamics. The nonlinear dependence of the GR rate equations on n, n_1, n_2 and $\mathcal{E}\equiv|\boldsymbol{\mathcal{E}}|$ gives rise to an S-shaped current-density field characteristic of the homogeneous steady state.

The current density $\boldsymbol{j}(\boldsymbol{B})$ in the presence of a magnetic field $\boldsymbol{B}$ normal to the current flow is written as

$$\boldsymbol{j}(\boldsymbol{B})=\frac{\boldsymbol{j}(0)+\mu\boldsymbol{B}\times\boldsymbol{j}(0)}{1+|\mu\boldsymbol{B}|^2}, \tag{1}$$

where μ is the electron mobility and $\boldsymbol{j}(0)$ is the current density for $B=0$, which is expressed within the drift-diffusion approximation as $\boldsymbol{j}(0)=e(n\mu\boldsymbol{\mathcal{E}}+D\nabla n)$, with the diffusion constant D.

The constitutive model equations are given by the rate equations for n, n_1, n_2, and the charge conservation equation $\nabla\cdot\boldsymbol{J}=0$ with $\boldsymbol{J}=\epsilon\dot{\boldsymbol{\mathcal{E}}}+\boldsymbol{j}$, where $\boldsymbol{J}$ is the total current density composed of the displacement current density $\epsilon\dot{\boldsymbol{\mathcal{E}}}$ and the conduction current density $\boldsymbol{j}(\boldsymbol{B})$.[11]

In order to solve these nonlinear space- and time-dependent equations self-consistently for a realistic two-dimensional sample geometry, we use an implicit finite element scheme.[28,29] To cope with the difficulties in the numerical treatment arising from the strong nonlinearity of the GR equations and the steep spatial gradients expected from the nature of breakdown phenomena, we have adopted a simulation algorithm based on a semi-implicit Euler scheme for time discretization with efficient time-step control.[11]

The simulated sample represents a square epitaxial GaAs layer with side lengths $L_x=L_z=0.02$ cm and thickness $L_y=1.4\times10^{-4}$ cm with point contacts in the center of two opposite sample edges, where the electron concentration is fixed to $n=5\times10^{15}$ cm^{-3}. This numerical value of the (Dirichlet) boundary condition at the contacts corresponds to the effective donor density $N_D^*=N_D-N_A$ (see material parameters in Table I). The simulations are not sensitive to this particular value as long as it is not chosen less than N_D^*, which is the minimum value required to supply enough electrons to model an Ohmic contact.

TABLE I. Material parameters for n-GaAs used in the simulations.

Parameter	Symbol	Value
Donor concentration	N_D	7.0×10^{15} cm^{-3}
Acceptor concentration	N_A	2.0×10^{15} cm^{-3}
Lattice temperature	T_L	4.2 K
Mobility	μ	1.0×10^{5} cm^2/Vs
Diffusion constant	D	$D=\mu k_B T_L/e$
Dielectric constant	ϵ	$10.9\epsilon_0$

III. SIMULATION OF CURRENT FILAMENTS

A. Nascence of filaments

Here we investigate the formation of a current filament upon application of a voltage ramp. Within 1 ps the voltage is linearly increased from 0 V to 0.48 V corresponding to an average electric field of $\mathcal{E}_{\rm av}=24$ V/cm which is above the threshold field for impurity breakdown, i.e., $\mathcal{E}_{\rm th}\approx 17$ V/cm, estimated from spatially homogeneous MC simulations.[9] A magnetic field is applied in the direction perpendicular to the sample plane pointing downwards with a strength of $B=5$ mT.

The dynamic processes of current filament formation under a transverse magnetic field are shown in Fig. 1. After the voltage is applied at the anode, a dipolelike electric field is formed quasi-instantaneously between the two point contacts inducing electron injection from the cathode. Then a charge carrier front is formed near the cathode ($x=0.02$ cm) and propagates towards the anode [A and B of Fig. 1(a)]. Though the carrier front is driven by impact ionization, it is not strong enough to affect carrier population in the shallow impurities. In other words, almost all the carriers in the bulk are still bound at the donor ground level, so the carrier concentration in the excited donor level n_2 is very low everywhere except for the vicinity of the Ohmic contacts [C of Fig. 1(a)]. The carrier density in the vicinity of the noninjecting anode contact is also increased by a weak impact ionization, since a relatively large fraction of the applied voltage drops at the junction between the n-type anode and the insulating bulk in a manner similar to a reversely biased n-p junction, leading to a higher electric field here. Note that the growth of the carrier front on the anode side, which is mainly driven by diffusion, has already been affected by the Lorentz force [B of Fig. 1(a)]. The electron temperature T_e is only slightly increased from the lattice temperature $T_L=4.2$ K in the area between the point contacts [D of Fig. 1(a)].

In order to conserve the total current density $\boldsymbol{J}$ longitudinally following from the charge conservation equation $\nabla\cdot\boldsymbol{J}=\boldsymbol{0}$, which is approximately given by $\boldsymbol{J}=en\mu\boldsymbol{\mathcal{E}}$, the electric field $\boldsymbol{\mathcal{E}}$ ahead of the carrier front, where the electron density n is still low, becomes higher than behind it. Hence impact ionization downstream is encouraged. When the injecting of the carrier front finally reaches the other front near the anode contact [A and B of Fig. 1(b)], most of the applied voltage is sustained here and the electric-field strength becomes high enough to trigger strong impact ionization from the donor ground level. This is visualized well by the sharp increase in the carrier population of the excited donor level there [C of Fig. 1(b)], which is not brought about by the direct transition from the donor ground level but by the enhancement of capture from the conduction band due to free carrier multiplication. The electron temperature, however, is not significantly increased yet [D of Fig. 1(b)].

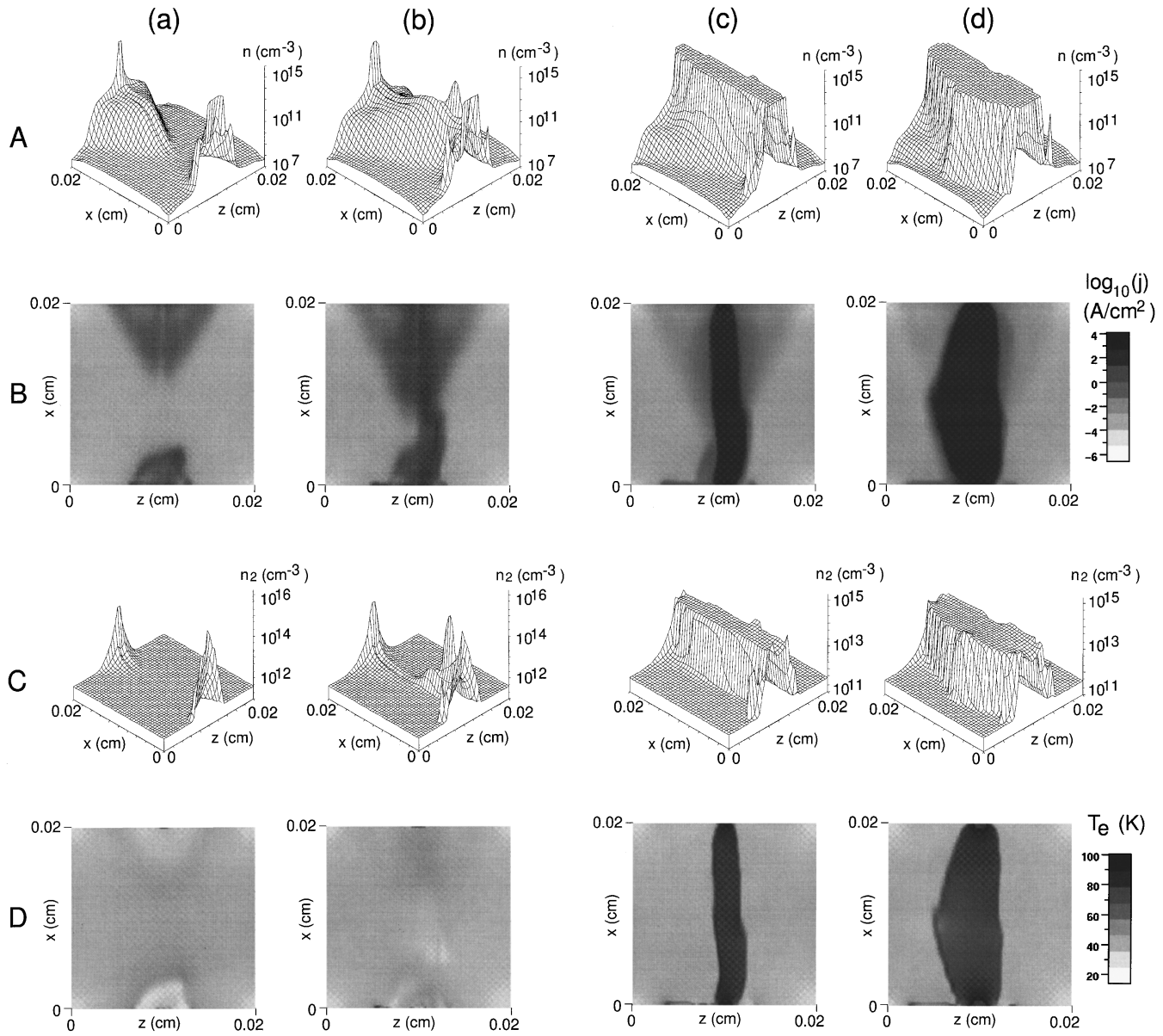

FIG. 1. Temporal evolution of (*A*) the electron density n, (*B*) the current density $|\boldsymbol{j}(x,z)|$, (*C*) the electron density $n_2(x,z)$ in the excited donor level, and (*D*) the electron temperature $T_e(x,z)$ as a function of the spatial coordinates x and z for a square sample with two point contacts at $B=5$ mT. (a) $t=0.5$ ns, (b) $t=1.0$ ns, (c) $t=1.6$ ns, (d) $t=2.5$ ns. The applied voltage $V=$ 0.48 V corresponds to an average field $\mathcal{E}_{\rm av}=$ 24 V/cm. Note that the cathode is at the top.

The increased free carrier concentration relaxes the electric field near the anode, then the high-field domain starts moving back from the anode to the cathode, again for the reasons of current conservation in a seesawlike mode.[10] Hence impact ionization propagates longitudinally, following the motion of the high-field domain, and multiplies the number of free carriers uniformly by several orders of magnitude, finally forming a thin homogeneous straight filament [*A* and *B* of Fig. 1(c)]. Inside the filament, the excited donor levels are also populated uniformly [*C* of Fig. 1(c)], whereas the ground level is almost depleted; this indicates that GR processes between the conduction band and the excited donor level become dominant. As a result the electron temperature strongly increases inside the filament [*D* of Fig. 1(c)], since impact ionization from the excited donor level (in contrast to the ground level) can no longer cool the electron temperature effectively due to the small relaxation energy involved.

In the next stage, the straight filament is gradually widened and bent in the direction of the Lorentz force [*A* and *B* of Fig. 1(d)]. The density of carriers trapped in the excited donor level is also shifted transversally with slightly increasing population towards the filament border [*C* of Fig. 1(d)]. On the other hand, the electron temperature slightly decreases in the expanded area of the bent filament [*D* of Fig. 1(d)]. This is because the average electric field becomes weaker as the distance from the central axis becomes larger, due to the point contact geometry inducing a dipolar field. In this area, the impact-ionization rate is also decreased, nonetheless, the filament still maintains a steep wall on this side

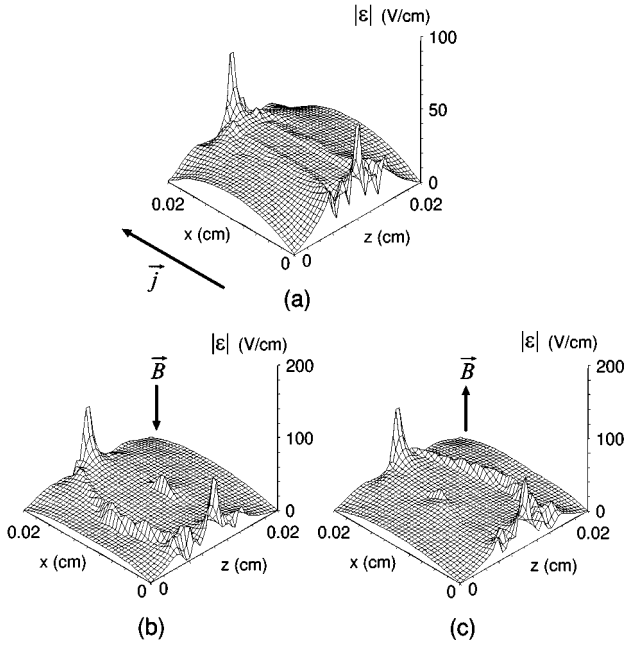

FIG. 2. Spatial distribution of electric-field strength $|\boldsymbol{\mathcal{E}}(x,z)|$ for (a) $B=0$, (b) $B=5$ mT, and (c) $B=-5$ mT at the quasi-steady-state ($t\approx 2.5$ ns), $V=0.48$ V. A magnetic field pointing downwards is defined as positive and upwards as negative.

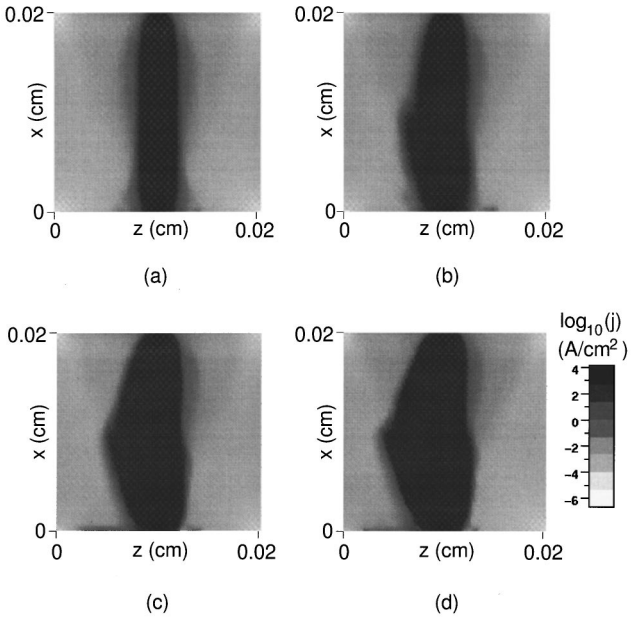

FIG. 3. Spatial patterns of current density $|\boldsymbol{j}(x,z)|$ for (a) $B=0$, (b) $B=2$ mT, (c) $B=5$ mT, and (d) $B=10$ mT at the quasi-steady-state ($t\approx 2.5$ ns), $V=0.48$ V. The width and curvature of filaments increase with magnetic-field strength.

[*A* of Fig. 1(d)], since the local electric field is very high at the filament border bent by the Lorentz force, as shown in the next section.

B. Lorentz-force effects

In order to confirm that the lateral growth of current filaments is attributed to the Lorentz force, the orientation of an applied magnetic field has been inverted in the simulations. We find that inverting the magnetic field generates a symmetric pattern of current flow with respect to the $z=0.01$ cm plane, as expected from the reversed Lorentz force. Figure 2 shows the spatial distribution of the electric field strength at $t=2.5$ ns, i.e., when a steady state is practically reached, for $B=0$ and $B=\pm 5$ mT, where a magnetic field pointing downwards is defined as positive and upwards as negative, and the cathode is always at the top. Compared with the symmetric distribution of the electric field for $B=0$, the fields exhibit strong asymmetry at opposite filament boundaries for $B=\pm 5$ mT. The electric fields at the filament borders pointing in the direction of the Lorentz force are much stronger than at the opposite borders. These asymmetric fields are in good agreement with asymmetric ridgelike structures observed by scanning laser microscopy under a transverse magnetic field.[8,21,22]

Spatial patterns of current filaments are compared for $B=0$, 2 mT, 5 mT, and 10 mT in the quasisteady state (Fig. 3). The width and curvature of the filaments become larger with increasing magnetic-field strength; this is expected from the increased Lorentz force and is similar to experiments.[8,22]

C. Current-time characteristics

The total current during the formation of current filaments is shown in Fig. 4 for different magnetic fields. The current-time characteristics consist of four stages corresponding to the formation processes of a current filament shown in (a)–(d) of Fig. 1: (a) low current state corresponding to a stage of carrier front creation and propagation from the cathode, (b) slight increase and stagnation in the current corresponding to the formation of a rudimentary filament followed by the backward motion of a high-field domain, (c) strong increase in the total current accompanied by the establishment of a homogeneous straight filament, and (d) almost saturated current with a filament bent by the Lorentz force. These basic processes have never been affected by applying magnetic fields with different strengths, on the other hand, it is remarkable in Fig. 4 that higher magnetic fields accelerate the transition from almost insulating to

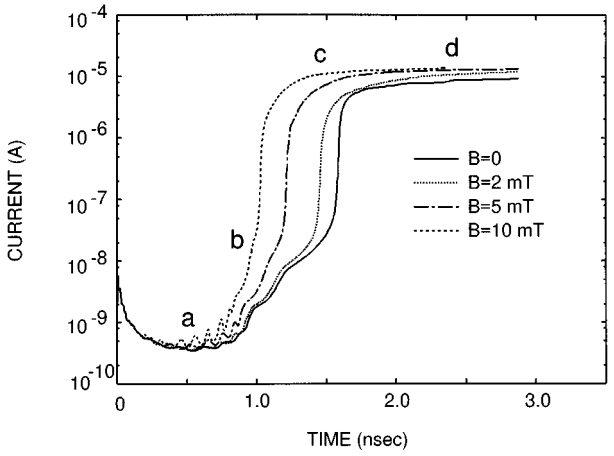

FIG. 4. Total current $I(t)$ during the formation of a filament for different magnetic fields. The letters (a)–(d) correspond to the stages of filament formation shown in (a)–(d) of Fig. 1.

highly conducting states. Similar $I(t)$ curves for $B=0$ have been measured in δ-doped samples.[30]

IV. DISCUSSION

In this section we discuss the physical processes involved in filament formation under a transverse magnetic field. A of Fig. 5 shows the cross sections of the modulus of the electric field strength with and without a magnetic field at $x=0.01$ cm, corresponding to each stage of filament formation shown in (a)–(d) of Fig. 1. Cross sections of the lateral electric field $\mathcal{E}_z$, and the corresponding space charge $\rho=e(N_D^*-n_1-n_2-n)=\epsilon\nabla\cdot\boldsymbol{\mathcal{E}}\approx\epsilon\partial\mathcal{E}_z/\partial z$, are also shown in B and C of Fig. 5, respectively, in the quasisteady state, where the shaded areas indicate the cross sections of electron concentration.

For $B=0$, the electric-field profile is completely symmetric with respect to the center of the sample ($z=0.01$ cm) during all stages of filament formation [(a) of Fig. 5A]. In the first stage the electric field exhibits a gentle peak at the middle of the sample due to the dipole-like electric field induced between the point contacts. After a charge carrier front passes by, the field profile then develops two maxima which arise from the lateral fields localized in the transition zone between high- and low-electron-density regions [(a) of Fig. 5B] and its formation is explained as follows. In the steady state, charge neutrality holds far from the filament borders since the negative charge of free electrons compensates positive ionized donors inside, and almost all donors are frozen out, i.e., neutral, outside the filament. In the transition zone, electrons tend to diffuse from high- to low-density regions leading to the weak carrier accumulation at the outside edge and the slight depletion at the inside edge of the filament walls. Hence charge neutrality is broken here because immobile ionized donors are left inside the filament borders [(a) of Fig. 5C]. The lateral electric field induced by this local space-charge dipole prevents the electrons from diffusing outwards, thus stabilizing the filament.

For $B=$ 5 mT, the electric field also retains an almost symmetric profile until the stage of a rudimentary filament ($t\approx$ 1.0 ns). However, once impurity breakdown sets in and a straight filament is growing, the electric field exhibits strong asymmetry between the opposite filament boundaries [(b) of Fig. 5A]. This arises from the asymmetric lateral field [(b) of Fig. 5B] and its origin can be explained by similar processes as for $B=$ 0. On the filament border pointing in the direction of the Lorentz force, the diffusion of the electrons out of the filament is enhanced. As a result more negative and positive space charges are generated by mobile electrons and by immobile ionized donors, respectively, on this border than for $B=0$ [(b) of Fig. 5C], giving rise to a strong local lateral field. The high-field border is shifted by the Lorentz force inducing impact ionization in the region behind it. Though the average electric-field strength inside the filament becomes weaker as the filament becomes wider due to the point-contact geometry, the free electron density is still high as long as the electric field is higher than the threshold field, $\mathcal{E}_h$, for impact ionization from the excited donor level, which is much smaller than that for the ground level. The lateral electric field serves as an attractive force compensating the outward Lorentz and diffusion forces, and if a balance holds between them, the filament border is stabilized under a transverse magnetic field.

On the other filament border, electrons diffusing outwards are impeded by the Lorentz force pointing into the opposite direction. Therefore less space charge and a weaker lateral field are created on this border than for $B=$ 0 [(b) of Fig. 5B and C]. This complementary action of lateral fields at the opposite boundaries can explain the asymmetric signals observed by laser scanning microscopy, where the signal of one filament border grows whereas the signal of the other border decays with increasing magnetic field.[21] We suggest that this asymmetric lateral field is also the source of the finite Hall voltage across the sample found in experiments[31] and it may play a crucial role in inducing chaotic oscillations.[27]

As explained above, spatial patterns of current filaments under a transverse magnetic field are determined by a local balance between the lateral diffusion current and the lateral drift current resulting from the lateral electric field which may be conceived as a superposition of the dipole field due to the space charge already present in the filament walls at $B=0$, and the Hall field. This physical picture is consistent with the reasoning developed previously for a one-dimensional model,[26] leading to transversally traveling filaments in the absence of a point-contact induced dipolar electric field. In our simulations, the filament border pointing in the direction of the Lorentz force is displaced transversally and the other border is almost fixed.

Another remarkable feature induced by applying a magnetic field is the acceleration of impurity breakdown (Fig. 4). A magnetic field does not directly affect the GR coefficients, but it affects the local field strength inside the filament. When no magnetic field is applied, the local electric field mainly consists of the longitudinal field $\mathcal{E}_x$, since no lateral field exists due to the local charge neutrality except for the filament boundaries as shown in (a) of Fig. 5B. On the other hand, when a magnetic field is applied transversally, a finite lateral Hall field $\mathcal{E}_z$ is generated inside the filament [(b) of Fig. 5(B)]. As a result the local electric-field strength should be always higher for $B\neq0$ than for $B=0$, because of $|\boldsymbol{\mathcal{E}}(\boldsymbol{B})|=\sqrt{\mathcal{E}_x^2+\mathcal{E}_z^2}\geq\mathcal{E}_x\approx|\boldsymbol{\mathcal{E}}(0)|$, where $\mathcal{E}_x$ is expected to be essentially the same with and without a magnetic field. The impact-ionization coefficients monotonically increase with local field strength. In particular, MC simulations show that impact ionization from the donor ground level, which plays a crucial role in the occurrence of impurity breakdown, drastically increases with the electric-field strength.[11] Therefore a magnetic field induces stronger impact ionization resulting in faster transitions from the low- to the high-conducting states. Although direct experiments on the switching times as a function of the magnetic field are not available, recent measurements of the frequency f of oscillating current filaments in the breakdown regime in GaAs epitaxial layers have demonstrated an increase of f with increasing B,[32] and thus appear to give indirect evidence for our theoretical prediction.

V. CONCLUSIONS

In this paper we have presented 2D simulations for the spatiotemporal dynamics of impurity breakdown in n-GaAs, accompanied by current filament formation, under the influence of a transverse magnetic field. Our simulations

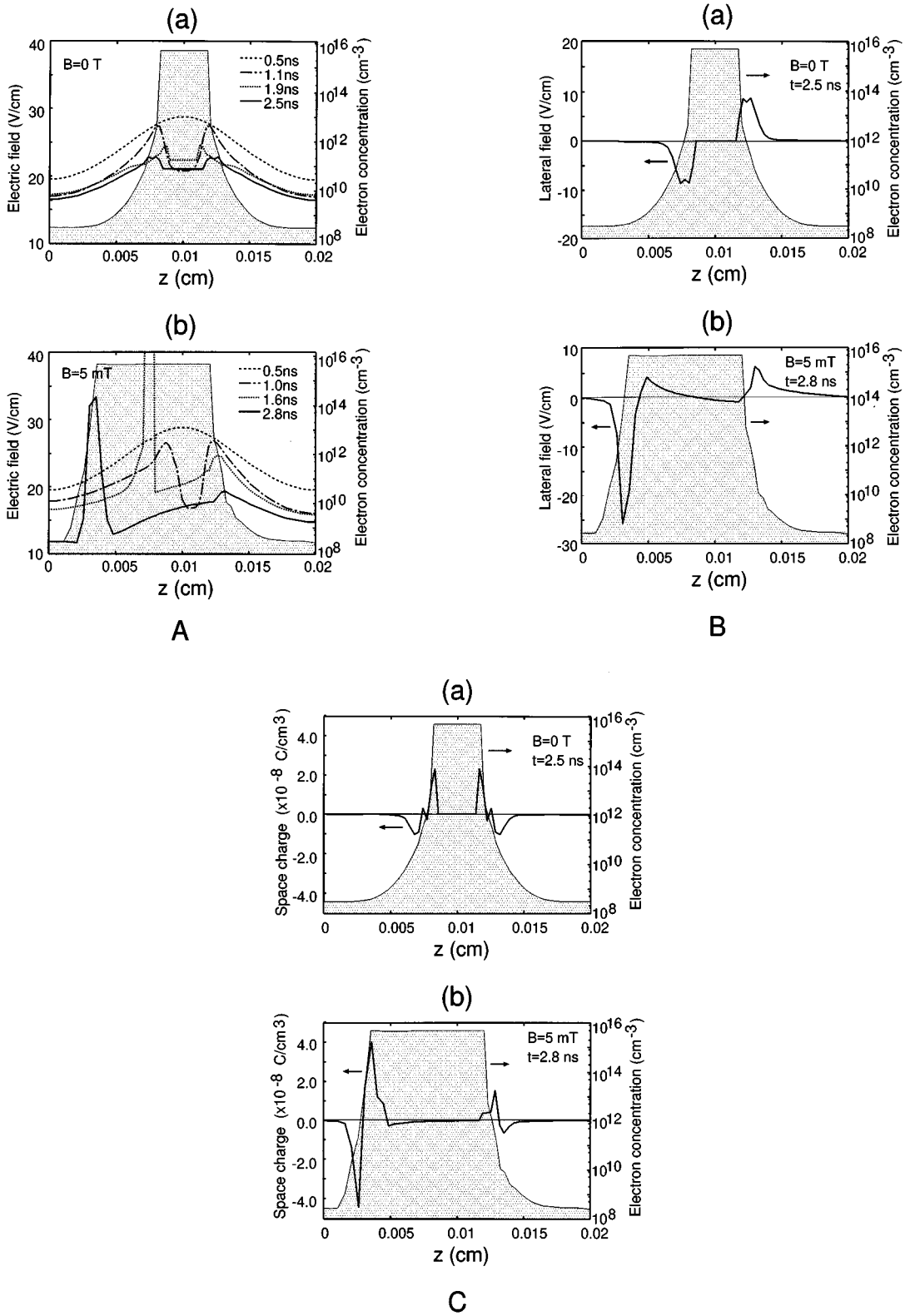

FIG. 5. Cross sections of (A) the electric field strength $|\boldsymbol{\mathcal{E}}(x,z)|$, ($B$) the lateral electric field $\mathcal{E}_z(x,z)$, and (C) the space-charge density in the middle between the two point contacts ($x=$ 0.01 cm) for (a) $B=$ 0 and (b) $B=$ 5 mT. The different times in (A) correspond to the stages of filament formation shown in (a)–(d) of Fig. 1. Shaded areas indicate the electron concentration in the quasisteady state ($V=0.48$ V).

show the following scenario for filament formation: (1) A charge-carrier front is formed at the cathode and propagates towards the anode, (2) a thin rudimentary filament is formed when the front has reached the anode, (3) the carrier density in the filament grows with strongly increasing electron temperature, (4) the fully developed filament is eventually widened and bent in the direction of the Lorentz force.

The width and curvature of filaments bent by the Lorentz

force increase with magnetic-field strength, and inverting the orientation of a magnetic field yields a symmetric spatial pattern. In addition, our simulations show that the electric-field profile exhibits strong asymmetry at opposite filament boundaries; this arises from the space charge accumulated asymmetrically at the filament walls. These features are in good agreement with recent experiments.

It has also been revealed by simulations that applying a transverse magnetic field accelerates impurity breakdown. This is because a transverse magnetic field induces a finite lateral Hall field inside the filament, thus increasing the modulus of the electric field. As a result transitions from almost insulating to highly conducting states are accelerated, since the impact-ionization probability rapidly increases with electric-field strength.

ACKNOWLEDGMENTS

We wish to thank H. Gajewski and R. Nürnberg from Weierstrass-Institut für Angewandte Analysis und Stochastik, Berlin for their help in adapting the 2D simulator ToSCA. We also thank W. Prettl, V. Novák, U. Margull, and W. Eberle from the University of Regensburg, H. Kostial from Paul-Drude-Institut, Berlin, and R. E. Kunz for helpful discussions.

*On leave from Opto-Electronics Research Laboratories, NEC Corporation, 34 Miyukigaoka, Tsukuba, Ibaraki, 305 Japan.

[1] E. Schöll, *Nonequilibrium Phase Transitions in Semiconductors* (Springer, Berlin, 1987).
[2] E. Schöll, Z. Phys. B **46**, 23 (1982); **48**, 153 (1982).
[3] E. Schöll, Phys. Rev. B **34**, 1395 (1986).
[4] G. Hüpper, K. Pyragas, and E. Schöll, Phys. Rev. B **47**, 15 515 (1993).
[5] T. Kuhn, G. Hüpper, W. Quade, A. Rein, E. Schöll, L. Varani, and L. Reggiani, Phys. Rev. B **48**, 1478 (1993).
[6] W. Quade, G. Hüpper, E. Schöll, and T. Kuhn, Phys. Rev. B **49**, 13 408 (1994).
[7] T. Christen, Phys. Rev. B **49**, 16 423 (1994).
[8] V. Novák, C. Wimmer, and W. Prettl, Phys. Rev. B **52**, 9023 (1995).
[9] B. Kehrer, W. Quade, and E. Schöll, Phys. Rev. B **51**, 7725 (1995).
[10] R. E. Kunz and E. Schöll, Z. Phys. B **99**, 185 (1996).
[11] M. Gaa, R. E. Kunz, and E. Schöll, Phys. Rev. B **53**, 15 971 (1996).
[12] K. Aoki, T. Kobayashi, and K. Yamamoto, J. Phys. Soc. Jpn. B **51**, 2372 (1982).
[13] S. W. Teitsworth, R. M. Westervelt, and E. E. Haller, Phys. Rev. Lett. **51**, 825 (1983).
[14] J. Peinke, A. Mühlbach, R. P. Huebener, and J. Parisi, Phys. Lett. **108A**, 407 (1985).
[15] D. Seiler, C. Littler, R. Justice, and P. Milonni, Phys. Lett. **108A**, 462 (1985).
[16] A. Brandl, T. Geisel, and W. Prettl, Europhys. Lett. **3**, 401 (1987).
[17] K. Yamada, N. Takara, H. Imada, N. Miura, and C. Hamaguchi, Solid State Electron. **31**, 809 (1988).
[18] K. Fujii, T. Ohyama, and E. Otsuka, Appl. Phys. A **48**, 189 (1989).
[19] J. Spinnewyn, H. Strauven, and O. Verbeke, Z. Phys. B **75**, 159 (1989).
[20] K. Mayer, J. Parisi, and R. Huebener, Z. Phys. B **71**, 171 (1988).
[21] A. Brandl, M. Völcker, and W. Prettl, Appl. Phys. Lett. **55**, 238 (1989).
[22] J. Spangler, B. Finger, C. Wimmer, W. Eberle, and W. Prettl, Semicond. Sci. Technol. **9**, 373 (1994).
[23] W. Eberle, J. Hirschinger, U. Margull, W. Prettl, V. Novák, and H. Kostial, Appl. Phys. Lett. **68**, 3329 (1996).
[24] W. Clauss, U. Rau, J. Peinke, J. Parisi, A. Kittl, M. Bayerbach, and R. P. Huebener, J. Appl. Phys. **70**, 232 (1991).
[25] G. Hüpper and E. Schöll, Phys. Rev. Lett. **66**, 2372 (1991).
[26] G. Hüpper, K. Pyragas, and E. Schöll, Phys. Rev. B **48**, 17 633 (1993).
[27] A. Brandl and W. Prettl, Phys. Rev. Lett. **66**, 3044 (1991).
[28] H. Gajewski, Z. Angew. Math. Mech. **2**, 101 (1985).
[29] R. E. Kunz, E. Schöll, H. Gajewski, and R. Nürnberg, Solid State Electron. **39**, 1155 (1996).
[30] H. Kostial, M. Asche, R. Hey, K. Ploog, and F. Koch, Jpn. J. Appl. Phys. **32**, 491 (1993).
[31] A. Brandl, W. Kröninger, W. Prettl, and G. Obermair, Phys. Rev. Lett. **64**, 212 (1990).
[32] U. Margull, Ph.D. thesis, University of Regensburg, 1996.